NANO LETTERS

LETTER

pubs.acs.org/NanoLett

Observation of Rabi Splitting from Surface Plasmon Coupled Conduction State Transitions in Electrically Excited InAs Quantum Dots

Brandon S. Passmore,[†] David C. Adams,[‡] Troy Ribaudo,[‡] Dan Wasserman,[‡] Stephen Lyon,[§] Paul Davids,[†] Weng W. Chow,[†] and Eric A. Shaner*[,†]

[†]Sandia National Laboratories, Albuquerque, New Mexico 87185-1086, United States

[‡]Department of Physics and Applied Physics, University of Massachusetts, Lowell, Massachusetts 01854, United States

[§]Department of Electric Engineering, Princeton University, Princeton, New Jersey 08544, United States

S *Supporting Information*

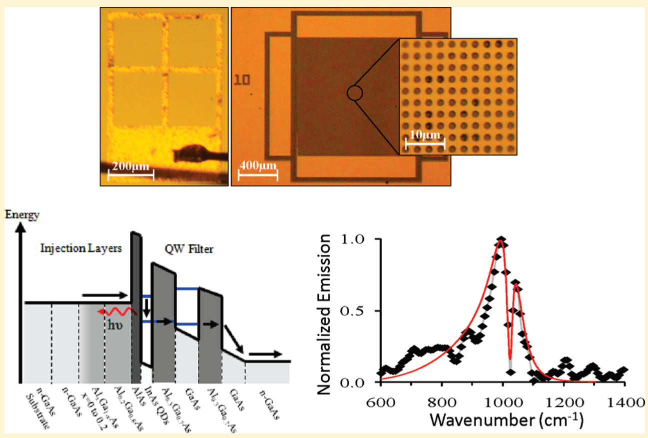

ABSTRACT: We demonstrate strong coupling between a surface plasmon and intersublevel transitions in self-assembled InAs quantum dots. The surface plasmon mode exists at the interface between the semiconductor emitter structure and a periodic array of holes perforating a metallic Pd/Ge/Au film that also serves as the top electrical contact for the emitters. Spectrally narrowed quantum-dot electroluminescence was observed for devices with varying subwavelength hole spacing. Devices designed for 9, 10, and 11 μm wavelength emission also exhibit a significant spectral splitting. The association of the splitting with quantum-dot Rabi oscillation is consistent with results from a calculation of spontaneous emission from an interacting plasmonic field and quantum-dot ensemble. The fact that this Rabi oscillation can be observed in an incoherently excited, highly inhomogeneously broadened system demonstrates the utility of intersublevel transitions in quantum dots for investigations of coherent transient and quantum coherence phenomena.

KEYWORDS: Midinfrared, plasmon, quantum dot, Rabi splitting, strong coupling, quantum cascade lasers

Rabi oscillations underlie all light—matter interactions involving coherent transients,[1] quantum interference[2,3] and (in the case of vacuum Rabi oscillations) cavity quantum electrodynamics.[4,5] Its demonstration is a first step toward achieving and studying effects such as self-induced transparency,[6] photon echoes,[7] or electromagnetically induced transparency[8] in a particular experimental platform. There is practical significance as well. The observation of Rabi oscillations signals a strong coupling between radiation and an active medium that can lead to new functionalities in devices. Examples include the feasibility of laser action at X-ray[9] or even γ-ray[10] wavelengths, the development of nonclassical light sources,[11] and the capability for fast, sensitive detection of biochemical agents using femtosecond adaptive spectroscopic techniques applied to coherent anti-Stokes Raman spectroscopy.[12]

The observation of Rabi oscillation or strong coupling in a semiconductor system is particularly significant.[13] On the one hand is the interesting physics arising from reproducing the atomic light—matter interaction effects in a physically more complex many-body environment.[14] On the other hand is the considerable application potential, because of the widespread use of optoelectronic devices in our daily lives. To date Rabi oscillation has been demonstrated by optically exciting nanostructures embedded in microcavities,[15,16] organic semiconductor microcavities,[17,18] organic molecules interacting with surface plasmons (SPs),[19] SP coupled CdSe nanocrystals,[20] and electrically injected polariton microcavity light-emitting diodes[21] and intersubband devices.[22] In this Letter, we report strong coupling in electrically excited semiconductor nanostructures. The experiments were performed on mid-infrared (mid-IR) emitting quantum-cascade-like structures utilizing self-assembled InAs quantum dots (QDs) in the device active region, whose intersublevel transitions are coupled to SP excitations. Evidence for Rabi oscillation is based on the observation of unambiguous splitting in the emission spectra, whose details are reproduced by calculations based on

Received: July 22, 2010
Revised: November 23, 2010

strong coupling between a SP field and an inhomogeneously broadened QD ensemble.

The InAs QDs were embedded in GaAs/AlGaAs quantum cascade-like heterostructures which were grown on n+ GaAs substrates. Optical transitions in these structures occur between discrete QD states with strong optical dipole matrix elements. The heterostructures were designed to maximize electron injection into an upper QD state and removal from the QD ground state. Figure 1 depicts a typical conduction band profile along the growth direction. A detailed account of the material growth and design characteristics is reported in an earlier publication.[23]

Two different device types were fabricated out of the QD emitter structures: the first with top metal contacts consisting of open areas (windows), to determine the electroluminescence spectra of large-area, uncoupled emitters (see Figure 2a), and the second with top contacts consisting of metal films with periodic hole arrays (meshes), to study electroluminescence from SP-coupled emitter structures (see Figure 2b). The hole arrays were designed for extraordinary optical transmission (EOT)[24,25] at 9, 10, 11, and 12 μm when deposited on an undoped GaAs substrate. Device fabrication involved standard processing techniques consisting of photolithography, metal deposition, and liftoff. Each mesh contact consisted of an annealed Pd/Ge/Au (30/45/150 nm) film with a square lattice of circular holes covering an area of 1 mm × 1 mm. The center-to-center hole spacings for the 9, 10, 11, and 12 μm wavelength mesh designs are 2.8, 3.0, 3.3, and 3.6 μm, respectively. The corresponding hole diameters are 1.4, 1.5, 1.6, and 1.8 μm. Figure 2 shows images (inset) of the window and mesh device designed for 10 μm emission.

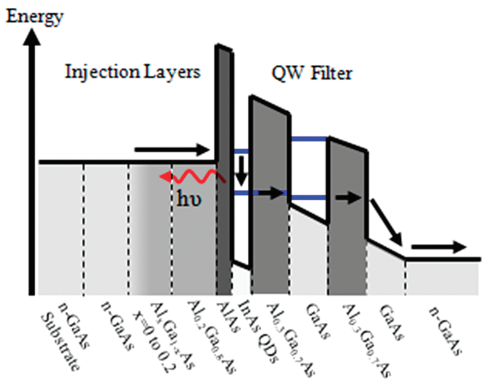

Figure 1. Electron confinement potential along the growth direction. With forward electrical bias, electrons flow from left to right. The electron injector is comprised of a graded $Al_xGa_{1-x}As$ ($x = 0-0.2$) region followed by a thin AlAs barrier next to which are InAs QDs. The QDs are capped with an $Al_{0.3}Ga_{0.7}As$ barrier. This arrangement pushes the QD ground state energy above the GaAs band edge. The collector filter is a single QW with subband band edge energies sandwiching those of the QD states.

Electroluminescence from the devices was collected at normal incidence using f/4 optics and measured with a Bruker V70 Fourier-transform IR spectrometer operating in amplitude modulation step-scan mode with a resolution of 32 cm^{-1}. The devices were mounted in a liquid nitrogen cooled cryostat. The applied current was pulsed at 40 kHz with a 40% duty cycle. The normalized 77 K electroluminescence spectra from the window-contacted devices and from the 10 μm mesh design are shown in panels a and b of Figure 2, respectively. Due to a weak response in the window-contacted devices, we biased many of them simultaneously and measured their combined emission. The broad band emission spans from 600 to 1300 cm^{-1} which is due to the QD size distribution. The application of a metal hole array would be expected to provide a band pass filtering effect when applied as a top contact to a light-emitting device. When the window and 10 μm mesh contact emission spectra in Figure 2 are compared, it is clear that the emission has been significantly narrowed in bandwidth and is centered near 1000 cm^{-1}. Upon closer inspection, within this narrow band emission a sharp null or splitting can be seen.

To learn about the spectral splitting, we first determine its location relative to the more familiar spectral features of a metallic hole array. Since the QD material is grown on doped GaAs substrates, it is not possible to perform direct transmission measurements. Complete spatial and spectral mapping of similar structures were performed in earlier investigations of metallic hole arrays,[26,27] in this wavelength range. On the basis of those results, we can use reflection measurements to correlate emission features with specific excitations of the hole arrays. To elaborate, we plot in Figure 2b, the normal-incident reflection of the 10 μm EOT mesh at a temperature of 77 K. Typically, reflection minimum and transmission maximum coincide in an EOT structure.[27] The correlation between the emission null with the expected energy for the SP implies that the dip in the emission spectra is most likely related to this plasmon mode at the metal/semiconductor interface.

The electroluminescence from all four sets of mesh-contact devices are displayed in Figure 3. For each device, the emission is centered close to the designed EOT transmission wavelength. Well-defined emission splittings near the middle of the expected passbands for the 9, 10, and 11 μm devices can be seen in panels

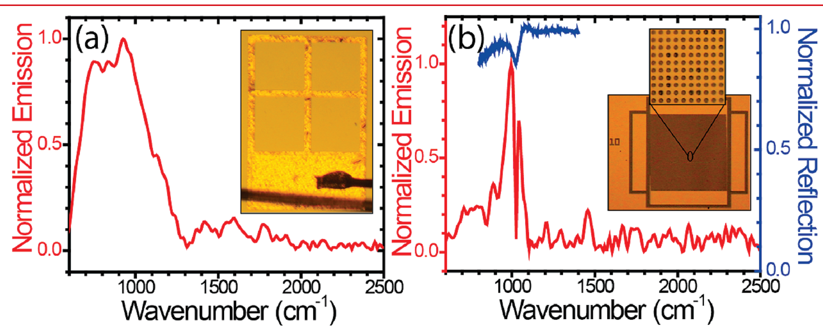

Figure 2. Quantum dot device spectral properties and geometry. The emission and device geometry (inset) are shown in (a) for the window contact device and in (b) for the 10 μm mesh device. The reflection spectrum of the mesh device is also included in (b). For the mesh contact, the surrounding metal as well as left and right metallic pads are not physically connected to the hole array.

dx.doi.org/10.1021/nl102412h | Nano Lett. XXXX, XXX, 000–000

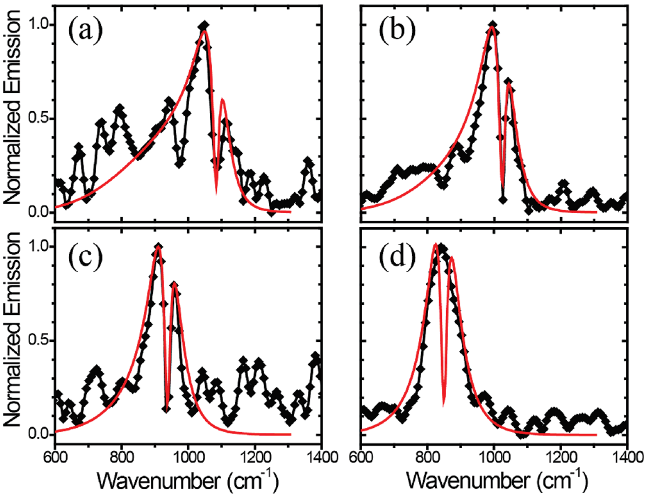

Figure 3. Electroluminescence spectra from (a) 9, (b) 10, (c) 11, and (d) 12 μm mesh-contact devices. The black dots (connected by gray lines) are from experiments and the red curves are from theory. Only the detuning between the SP resonance and the center of QD distribution is varied to produce the fits for different devices.

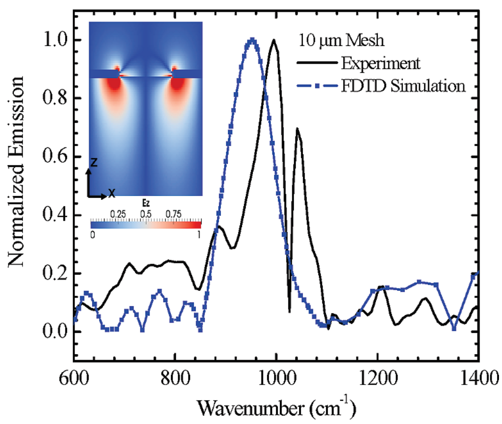

Figure 4. Finite-difference time-domain simulation results of the 10 μm mesh design with an electric dipole source plane in place of the InAs quantum dots and the 10 μm mesh experimental data. The inset shows the z-component of the electric field and depicts the surface plasmon mode at the metal/GaAs interface occurring at 945 cm^{-1}.

a−c of Figure 3, respectively. The splitting is not observed in the 12 μm mesh device emission shown in Figure 3d.

In order to understand the origin of the splitting effect, the mesh structures were simulated using a classical electric dipole source plane to represent the electroluminescent quantum dot layer. The simulated emission spectrum for the QD emitters was obtained using a finite-difference time-domain (FDTD) method for solving Maxwell's equations. For the simulations, the cavity structure consisted of a Au EOT mesh and the matrix surrounding the emitter layer was GaAs. The underlying doped GaAs substrate was treated using a Drude model with a carrier density of 3×10^{18} cm^{-3} and a damping time of 200 fs. As shown in Figure 4, the peak in the simulated normal incidence emission corresponds to a SP mode occurring at roughly 945 cm^{-1} (10.6 μm) between the mesh and GaAs interface. The 9,11, and 12 μm mesh geometries were simulated as well and yielded similar results. Though the experimentally observed narrowing of the emitted spectra was reproduced in the FDTD simulations, no splitting of the simulated emission peak was observed . This demonstrates that the spectral signatures of our devices that indicate strong coupling of the QD emitter layer to the cavity SP mode are absent in this simple classical model. While adding resonant coupling to the QD emitter layer can be included phenomenologically as a Lorentz oscillator, the oscillator strengths, resonant frequency, and resonance line width should be computed within a quantum mechanical framework.

To explore further, we considered a quantum mechanical approach that describes the splitting and associated asymmetry in the emission peaks, as well as reproducing the measured spectra with minimal adjustment of parameters. Our approach models an ensemble of QDs that emit radiation via spontaneous emission while strongly interacting with an electric field of a plasmon mode. For this description, the system Hamiltonian is[28]

$$H = \sum_{\omega} \hbar\omega |a_\omega\rangle\langle a_\omega| + \sum_{v} \hbar v c_v{}^{+} c_v + \sum_{\omega,v} \mu(|a_\omega\rangle\langle b_\omega| + |b_\omega\rangle\langle a_\omega|)E(z,t) \tag{1}$$

where $|a_\omega\rangle$ and $|b_\omega\rangle$ are two QD electronic levels, c_v and $c_v{}^{+}$ are photon annihilation and creation operators, ω and v are the QD transition and photon frequencies, respectively, μ is the dipole matrix element, and $E(z, t)$ includes both the classical plasmon field and the quantized spontaneous emission field. By solving this system (see Supporting Information for details), we derived an expression for the power emission of the plasmon coupled ensemble described by eqs 2−4.

$$S(v) = \int_0^\infty d\omega\, P(\omega) \left(\frac{g_\omega \Omega_R}{\Omega_R{}'}\right)^2 \gamma \left\{ \frac{\eta(\Omega_R{}')}{\gamma + i(2v - \Omega - \omega + \Omega_R{}')} + \frac{\eta(-\Omega_R{}')}{\gamma + i(2v - \Omega - \omega + \Omega_R{}')} \right\} + c.c. \tag{2}$$

$$\eta(\Omega_R') = \frac{1}{\gamma^2 + (\Delta - \Omega_R{}')^2} - \frac{1}{[\gamma - i(\Delta - \Omega_R{}')][\gamma + i(\Delta + \Omega_R{}')][\gamma + i\Omega_R{}']} \tag{3}$$

$$\Omega_R' = \sqrt{\Omega_R{}^2 + \Delta^2} \tag{4}$$

Here, $P(\omega)$ is the inhomogeneously broadened QD distribution obtained by fitting the emission spectra from a window device with a Gaussian line shape having a width of $\Delta_{inh} = 2.64 \times 10^{13}$ s^{-1}, $\Delta = \Omega - \omega$ where Ω is the plasmon mode eigenfrequency, γ is the dephasing, Ω_R is the on resonance Rabi frequency, and Ω'_R is the detuned Rabi frequency.

To reproduce the 10 μm hole array spectra, we use eq 4 with $\Omega_R = 4.71 \times 10^{12}$ s^{-1} and $\gamma = 1.26 \times 10^{12}$ s^{-1} (see solid red curve in Figure 3b). To match the absolute wavenumber of the experimental data, we take the center of the QD distribution to be $\omega_0 = 1.52 \times 10^{14}$ s^{-1} and the detuning between the plasma resonance and QD distribution center is $\Delta_0 = \Omega - \omega_0 = 4.15 \times 10^{13}$ s^{-1}. The assumed Rabi frequency implies an electric field of 3 kV/cm at the plasmon resonance which is consistent with our experiment. A dephasing rate of $\gtrsim 10^{12}$ s^{-1} is predicted for both

dx.doi.org/10.1021/nl102412h | *Nano Lett.* XXXX, XXX, 000–000

ground and excited state transitions in deep QDs such as an InAs QD at electron densities $\sim 10^{11}$ cm^{-2}, with roughly equal contributions from electron−electron and electron−phonon scattering at 300 K.[29,30] Our measurements with similar devices indicate mid-IR plasmon resonance linewidths to be of roughly similar magnitude (~2 meV).[27]

The other plots in Figure 3 show the fit between theory and experiment for the 9, 11, and 12 μm devices. In the calculation, we changed only the detuning (Δ_0) between the plasmon frequency and QD distribution in order to center the calculated spectra with the experimental data. Panels a and c of Figure 3 show good agreement between theory and experiment, especially in terms of the change in the ratio of the emission peak amplitudes. Since the agreement is achieved by adjusting only one parameter, the model further supports our description of the experiment. Figure 3d shows that we are unable to reproduce the spectral null in the 12 μm device. This may be due to an increase in free carrier absorption at longer wavelengths from the doped substrate. In past work with metallic hole arrays on highly doped InSb, we observed broadening in the transmission spectra as the doping density increased when the impinging field interacts with the doped layer.[31] The broadening arises from an increase in nonradiative damping of the SPs by free-carrier absorption. The underlying doping of the substrate used for material growth in the present samples is $\sim 10^{18}$ cm^{-3}, which is comparable to the level where increased broadening was previously observed in similar structures and wavelength range. In addition, at longer wavelengths the penetration depth of SPs increases which, consequently, increases the interaction between the field and doped substrate.

Several factors contribute to the presence of strong coupled emission in our plasmonic system. First, by working in the mid-IR, we increase the overlap of the SP fringing field and the active material. The SP fringing field penetration depth into the semiconductor is typically on the order of half of the wavelength in the material.[32] If the QD layer is grown close enough to the metal/GaAs interface, a strong electrodynamical coupling between the QDs and the SPs can occur. Since the QD layer was grown ~130 nm below the surface, it is well within the fringing field of the SPs. Second, the dipole matrix element of an interconduction−state transition is significantly larger than an electron−hole transition. Third, the electron-injection scheme, which is similar to that of quantum well (QW) quantum cascade lasers, preferentially populates the QD upper emitting state, increasing likelihood of exciting a pure quantum state. However, using intersubband transitions in QDs instead of intersubband transitions in a QW can be advantageous as the dephasing rate in our devices may be slower because of mismatch between longitudinal optical phonon energy and energy separations of the discrete QD levels.

In conclusion, we observed strong light−matter interaction in mid-IR emission from electrically pumped, self-assembled InAs quantum dots in a quantum-cascade-like device. The surface-normal emission is from transitions between conduction states in the InAs QDs. For each device, the peak emission wavelength is selected by the subwavelength periodicity of a lattice of apertures on a metallic film that also serves as an electrical contact. The electroluminescence spectra for devices emitting at the 9−11 μm wavelength range show distinct spectral splittings that we identify as arising from Rabi oscillations. This claim is supported by a calculation of spontaneous emission from interconduction-state transitions of a QD ensemble interacting strongly with an electric field of a plasmon mode. The coupling of semiconductor nanostructures to plasmonic elements is scientifically interesting and technologically important. Our demonstration of Rabi oscillation proves that interconduction-state transitions in self-assembled QD samples can serve as a platform for quantum-optics experiments and opens up the possibility of nonclassical long-wavelength plasmonic optoelectronic devices.

ASSOCIATED CONTENT

Supporting Information. Additional details. This material is available free of charge via the Internet at http://pubs.acs.org.

AUTHOR INFORMATION

Corresponding Author
*E-mail: eashane@sandia.gov.

ACKNOWLEDGMENT

This work was supported by the U.S. Department of Energy, Office of Science, Office of Basic Energy Sciences through the Energy Frontier Research Center (EFRC) for Solid-State Lighting Science. This work was performed, in part, at the Center for Integrated Nanotechnologies, a U.S. Department of Energy, Office of Basic Energy Sciences user facility. Sandia National Laboratories is a multiprogram laboratory operated by Sandia Corporation, a Lockheed-Martin Company, for the U.S. Department of Energy under Contract No. DE-AC04-94AL85000.

REFERENCES

(1) Brewer, R. G.; Hahn, E. L. *Phys. Rev. A* **1975**, *11*, 1641–1649.
(2) Zibrov, A. S.; Lukin, M. D.; Nikonov, D. E.; Hollberg, L.; Scully, M. O.; Velichansky, V. L; Robinson, H. G. *Phys. Rev. Lett.* **1995**, *75*, 1499–1502.
(3) Harris, S. E.; Yamamoto, Y. *Phys. Rev. Lett.* **1998**, *81*, 3611–3614.
(4) Haroche, S; Kleppner, D. *Phys. Today* **1989**, 24–30.
(5) Berman, P. R. *Cavity Quantum Electrodynamics*; Academic: Boston, 1994.
(6) McCall, S. L; Hahn, E. L. *Phys. Rev.* **1969**, *183*, 457–485.
(7) Abella, I. D.; Kurnit, N. A; Hartmann, S. R. *Phys. Rev.* **1966**, *141*, 391–406.
(8) Harris, S. E. *Phys. Today* **1997**, *50*, 36–42.
(9) Suckewer, S.; Skinner, C. H.; Milchberg, H.; Keane, C.; Voorhees, D. *Phys. Rev. Lett.* **1985**, *55*, 2409–2412.
(10) Kocharovskaya, O. A. *Laser Phys.* **1995**, *5*, 284–291.
(11) Slusher, R. E.; Hollberg, L. W.; Yurke, B.; Mertz, J. C.; Valley, J. F. *Phys. Rev. Lett.* **1985**, *55*, 1753–1756.
(12) Scully, M. O.; Kattawar, G. W.; Lucht, R. P.; Opatrny, T.; Pilloff, H.; Rebane, A.; Sokolov, A. V.; Zubairy, M. S. *Proc. Natl. Acad. Sci. U.S.A.* **2002**, *99*, 10994–11001.
(13) Cundiff, S. T.; Knorr, A.; Feldmann, J.; Koch, S. W.; Gobel, E. O.; Nickel, H. *Phys. Rev. Lett.* **1994**, *73*, 1178–1181.
(14) Khitrova, G.; Gibbs, H. M.; Jahnke, F.; Kira, M.; Koch, S. W. *Rev. Mod. Phys.* **1999**, *71*, 1591–1639.
(15) Houdré, R.; Weisbuch, C.; Stanley, R. P.; Oesterle, U.; Pellandini, P.; Ilegems, M. *Phys. Rev. Lett.* **1994**, *73*, 2043–2046.
(16) Khitrova, G.; Gibbs, H. M.; Kira, M.; Koch, S. W.; Scherer, A. *Nat. Phys.* **2006**, *2*, 81–90.
(17) Lidzey, D. G.; Bradley, D. D. C.; Skolnick, M. S.; Virgili, T.; Walker, S.; Whittaker, D. M. *Nature* **1998**, *395*, 53–55.
(18) Bellessa, J.; Bonnand, C.; Plenet, J. C.; Mugnier, J. *Phys. Rev. Lett.* **2004**, *93*, No. 036404.

(19) Dintinger, J.; Klein, S.; Bustos, F.; Barnes, W. L.; Ebbesen, T. W. *Phys. Rev. B* **2005**, *71*, No. 035424.
(20) Gómez, D. E.; Vernon, K. C.; Mulvaney, P.; Davis, T. J. *Nano Lett* **2010**, *10*, 274–278.
(21) Tsintzos, S. I.; Pelekanos, N. T.; Konstantinidis, G.; Hatzopoulos, Z.; Savvidis, P. G. *Nature* **2008**, *453*, 372–375.
(22) Jouy, P.; Vasanelli, A.; Todorov, Y.; Sapienza, L.; Colombelli, R.; Gennser, U.; Sirtori, C. *Phys. Rev. B* **2010**, *82*, No. 045322.
(23) Wasserman, D.; Ribaudo, T.; Lyon, S. A.; Lyo, S. K.; Shaner, E. A. *Appl. Phys. Lett.* **2009**, *94*, No. 61101.
(24) Ebbesen, T. W.; Lezec, H. J.; Ghaemi, H. F.; Thio, T.; Wolff, P. A. *Nature* **1998**, *391*, 667–669.
(25) Wasserman, D.; Shaner, E. A.; Cederberg, J. G. *Appl. Phys. Lett.* **2007**, *90*, No. 191102.
(26) Ribaudo, T.; Adams, D. C.; Passmore, B.; Shaner, E. A.; Wasserman, D. *Appl. Phys. Lett.* **2009**, *94*, No. 201109.
(27) Ribaudo, T.; Passmore, B.; Freitas, K.; Shaner, E. A.; Cederberg, J. G.; Wasserman, D. *Opt. Express* **2009**, *17*, 666.
(28) Scully, M. O.; Zubairy, M. S. *Quantum Optics*; Cambridge University Press: Cambridge, 1977.
(29) Schneider, H. C.; Chow, W. W.; Koch, S. W. *Phys. Rev. B* **2004**, *70*, No. 235308.
(30) Lorke, M.; Chow, W. W.; Nielsen, T. R.; Seebeck, J.; Gartner, P.; Jahnke, F. *Phys. Rev. B* **2006**, *74*, No. 035334.
(31) Passmore, B. S.; Allen, D. G.; Vangala, S. R.; Goodhue, W. D.; Wasserman, D.; Shaner, E. A. *Opt. Express* **2009**, *17*, 10223–10230.
(32) Barnes, W. L.; Dereux, A.; Ebbesen, T. W. *Nature* **2003**, *424*, 824.